


Validation of pressure drop prediction and bed generation of fixed-beds with complex particle shapes using discrete element method and computational fluid dynamics

Nico Jurtz¹  | Gregor D. Wehinger² | Urvashi Srivastava³ | Tobias Henkel³ | Matthias Kraume¹

¹Chair of Chemical and Process Engineering, Technische Universität Berlin, Berlin, Germany

²Chemical and Electrochemical Process Engineering, Technische Universität Clausthal, Clausthal-Zellerfeld, Germany

³Clariant Corporation, BU Catalysts, Louisville, Kentucky

Correspondence

Nico Jurtz, Chair of Chemical and Process Engineering, Technische Universität Berlin, Fraunhoferstr. 33-36, 10587 Berlin, Germany. Email: nico.jurtz@tu-berlin.de

Funding information

Clariant

Abstract

Catalytic fixed-bed reactors with a low tube-to-particle diameter ratio are widely used in industrial applications. The heterogeneous packing morphology in this reactor type causes local flow phenomena that significantly affect the reactor performance. Particle-resolved computational fluid dynamics has become a predictive numerical method to analyze the flow, temperature, and species field, as well as local reaction rates spatially and may, therefore, be used as a design tool to develop new improved catalyst shapes. Most validation studies which have been presented in the past were limited to simple particle shapes. More complex catalyst shapes are supposed to increase the reactor performance. A workflow for the simulation of fixed-bed reactors filled with various industrially relevant complex particle shapes is presented and validated against experimental data in terms of bed voidage and pressure drop. Industrially relevant loading strategies are numerically replicated and their impact on particle orientation and bed voidage is investigated.

KEYWORDS

bed voidage, fixed-bed reactor, numerical modeling, particle orientation, pressure drop

1 | INTRODUCTION

Syngas is feedstock for many important chemical processes like methanol and ammonia synthesis, the production of aldehydes by oxo synthesis, and the generation of hydrocarbons by the Fischer-Tropsch process. Common routes for syngas production are heterogeneous catalytic reforming processes, for example, steam and dry reforming of methane.¹ Because of the highly endothermic or exothermic nature of these reactions, tubular reactors consisting of numerous fixed-beds with a low tube-to-particle diameter ratio N are widely used. They are characterized by an intensified radial heat transfer and a low pressure drop. However, in this reactor type the assumption of a homogeneous

radial void fraction distribution is not valid and local flow phenomena play an important role. This leads to a strong interplay between bed morphology, fluid dynamics, heat and mass transfer, and therefore, the reactor performance itself.

When it comes to process intensification, the probably most obvious way to improve the overall process is the testing of different catalyst shapes. The ideal particle shape has to satisfy multiple objectives: a high active catalytic surface, low pressure drop, low axial dispersion, and a good radial heat transfer characteristic. Several authors investigated the effect of the particle shape on reactor performance and life expectation theoretically and experimentally. Bruno et al² compared multi-hole cylinders with Raschig rings theoretically and found for

This is an open access article under the terms of the Creative Commons Attribution License, which permits use, distribution and reproduction in any medium, provided the original work is properly cited.

© 2020 The Authors. *AIChE Journal* published by Wiley Periodicals, Inc. on behalf of American Institute of Chemical Engineers.

multi-hole cylinders a two times longer maintenance interval until the catalyst needs to be replaced and a significantly increased life expectation for the reactor tubes. In their comprehensive review paper Sie and Krishna³ discuss several aspects regarding the impact of particle shape on reactor performance and found that the right choice of particle shape is a multi-objective optimization problem to solve the complex trade-off between low pressure drop, high surface-to-volume ratio, high specific reaction rate, low manufacturing cost, and high particle strength. Afandzadeh and Foumeny⁴ give in their work special attention to the impact of particle shape on bed morphology. They compare spheres, cylinders, Raschig rings, Lessing rings, and cross web cylinders regarding their active surface per unit volume while particle aspect ratio and inner-to-outer diameter ratio is varied. For cylinders they suggest an aspect ratio of $(h/d_p) = 1$, while for Raschig rings, Lessing rings, and cross web cylinders an optimum design range of $0.75 \leq (h/d_p) < 1.50$ and $0.4 < (d_{p,i}/d_{p,o}) < 0.8$ was identified. This leads to 20–30% extra surface area for Raschig rings compared to cylinders. Compared to the equivalent Raschig rings an increase in surface area of 10–27% can be seen for Lessing rings. This can be further increased by 16% if cross web cylinders are used. For steam reforming Kagyrmanova et al⁵ found in their theoretical optimization study that catalyst height and diameter have an opposed effect on conversion when holed cylinders are used. They propose particles with a high aspect ratio $((h/d_p) \approx 1.5)$ and a low diameter by considering the resulting pressure drop as limiting factor. Hartmann et al⁶ promote in their experimental work the use of perforated porous spherical particles and justify this with a significantly reduced pressure drop by only slightly reducing the conversion of methane steam reforming in comparison to 7-hole cylinders. The latter particle shape used for steam reforming was also investigated by Franczyk et al.⁷ They studied the influence of aspect ratio, hole diameter and tube-to-particle diameter ratio on relative activity, relative gas load, pressure drop, and wall temperature theoretically. The authors propose an aspect ratio of one, a tube-to-particle diameter ratio $N \geq 5$, and a hole-to-cylinder cross-section area ratio of 0.30–0.37. Karthik and Buwa⁸ used particle-resolved computational fluid dynamics (CFD) to investigate the impact of different particle shapes on the reactor performance for four industrially important solid-catalyzed gas-phase reactions. They found that, with increasing particle surface area, pressure drop increases while intra-particle temperature and concentration gradients decrease. The authors show that particle shape significantly impacts reactor performance. However, the overall efficiency depends on several factors as mass transfer limitation and reaction equilibrium. Therefore, the optimal particle shape was found to be dependent on the chemical reaction that is considered.

The relatively low number of experimental work in that field is explainable by the high costs and required time that is needed to conduct the experiments. Furthermore, the knowledge gain by experimental results is limited, since they are most often based on inlet-outlet measurements only. Therefore, in the last twenty years many researchers developed and used particle-resolved CFD simulations to get a better understanding of fluid dynamics and transport processes inside fixed-bed reactors. Particle-resolved CFD is an almost first-

principle modeling approach where the whole reactor including the interstices and if needed also the particles are spatially discretized and conservation equations are solved. Comprehensive reviews of this method can be found in Dixon et al⁹ and Jurtz et al.¹⁰

For simple particle shapes like spheres, cylinders, and Raschig rings many authors validated the particle-resolved CFD method against experimental results or correlations in terms of bed voidage,^{11–15} pressure drop,^{14,16–18} and temperature and species profiles.^{19–21} However, for more complex particle shapes only few publications exist. Caulkin et al generated packings of 4-hole cylinders,²² pall rings,¹³ and trilobes²³ numerically and compared the radial void fraction distribution with experimental data. For 4-hole cylinders and trilobes the numerical results were in good agreement with experimental data. For pall rings the void fraction was underestimated and only a fair agreement was found. Boccardo et al¹⁶ investigated a small sample of a trilobe packing and were able to find good agreement for the calculated pressure drop in comparison to Ergun's equation for low Reynolds numbers ($Re_p < 100$). However, increasing deviations were observed for higher Reynolds numbers.

In order to make particle-resolved CFD a design tool for new particle shapes the currently existing lack of experimental validation needs to be fixed. In this work, packings of different complex particle shapes with inner voids and outer surface structure are numerically generated using DEM and the pressure drop is calculated by CFD simulations. It is shown that a precise representation of the bed morphology is basis for a predictive CFD simulation. Therefore, special emphasis is given to the aspect of numerical packing generation and a method is presented that improves the match between experimentally and numerically generated packings by calibrating the static friction coefficient.²⁴ In industrial applications, very often special loading devices are used when the reactor is filled with particles. For the first time the impact of a special loading device, which is often used in industry, is considered and its impact on particle orientation and bed voidage is investigated.

2 | MATERIAL AND METHODS

2.1 | Experimental measurements

Experimental measurements were conducted in cylindrical reactor tubes with an inner diameter of $D = 101.6$ mm and $D = 152.4$ mm. Four different particle shapes were investigated. The shapes and their dimensions are depicted in Figure 1 and Table 1. Besides Raschig rings (RR) with almost equilateral dimensions, three more complex shapes were studied: two different types of 10-hole cylinders low pressure drop particle (LDP) with different aspect ratios $((h/d_p) \approx 0.62$ and $(h/d_p) \approx 0.81)$ and a 10-hole cylinder with an outer floral-type surface structure floral design (FD). The fronts of LDP and FD are completed by a small dome.

A loading procedure that is often applied in industrial applications was used: as depicted in Figure 2a a CATCADE™ reformer loading device by Cat Tech® is used for filling. The device is placed in central position inside the reactor tube, as shown in Figure 2b,

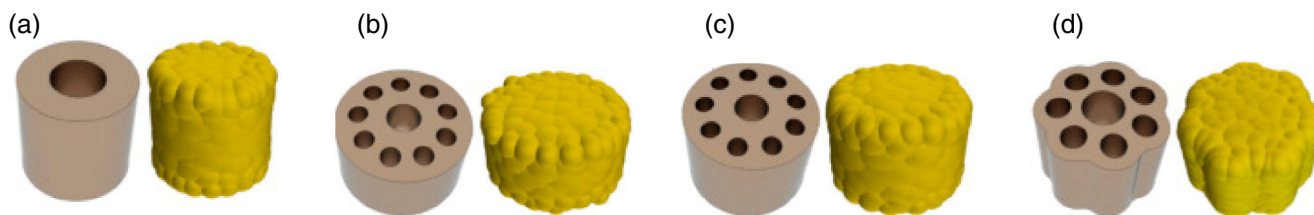


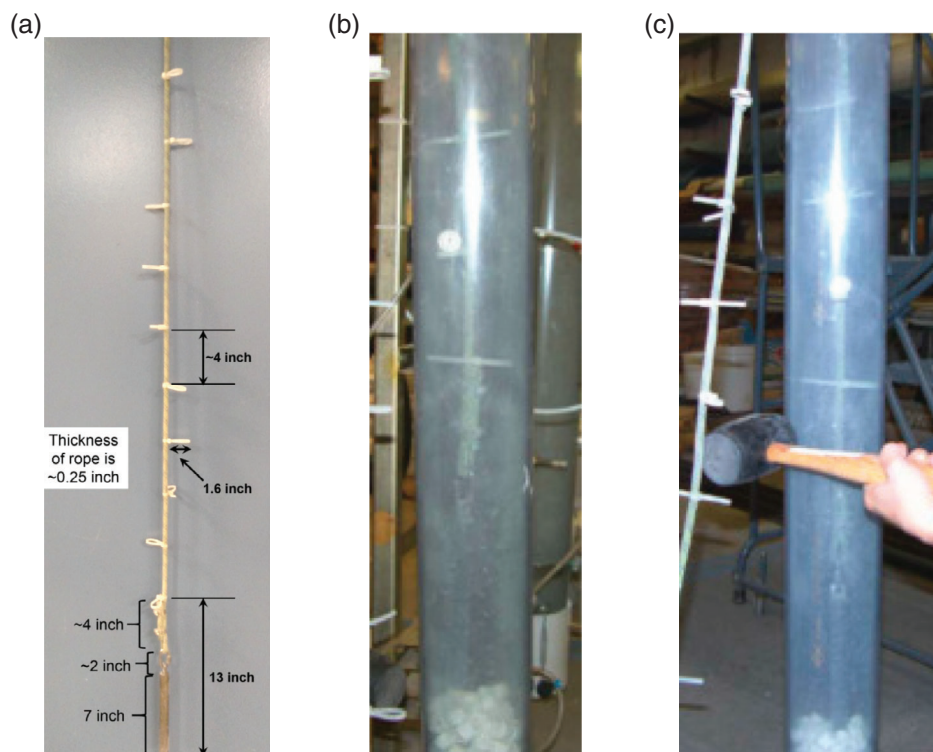
FIGURE 1 Investigated particle shapes and its DEM composite-particle representation: (a) Raschig ring (RR), (b) 10-hole cylinder 19 × 12 (LDP 19 × 12), (c) 10-hole cylinder 19 × 16 (LDP 19 × 16), and (d) 8-hole cylinder with floral design (FD). DEM, discrete element method [Color figure can be viewed at wileyonlinelibrary.com]

TABLE 1 Dimensions of the investigated particle shapes

	RR	LDP 19 × 12	LDP 19 × 16	FD
Outer diameter (mm)	16.55	20.66	19.71	20.46
Particle height (mm)	16.15	12.71	15.90	16.04

Abbreviation: RR, Raschig rings.

FIGURE 2 Experimental loading strategy. (a) CATCADE™ reformer loading device by Cat Tech®. (b) Loading device inside the reactor tube during filling process. (c) Hammering for artificial bed densification [Color figure can be viewed at wileyonlinelibrary.com]



and particles are poured from the top into the reactor until half of the tube is filled. Afterwards, the bed is densified by hammering against the reactor wall for 30 s as shown in Figure 2c. This procedure is repeated once. During the loading process the CATCADE™ device is moved upwards to prevent that it immerses into the bed. The loading device is used to reduce particle velocities and to prevent them from damage during the filling process. Furthermore, it is designed to reduce the variance in packing morphology, and therefore, variance in pressure drop between different reformer tubes. The overall aim is a reduced turnaround time for the filling process in industrial applications. The bed voidage is determined

by counting the particles that are needed to reach a specified bed height:

$$\varepsilon = 1 - \frac{\sum_i V_{p,i}}{\frac{\pi}{4} D_i^2 H} \quad (1)$$

The pressure drop measurements were conducted by blowing air at ambient conditions through the fixed-bed from top to bottom. The inlet flow rate is set by using a needle valve and controlled by

measuring the pressure difference before and after an orifice plate using HD750 differential pressure manometer by *Extech Instruments*. The pressure drop across the sample bed is measured using HHP-2081 digital manometer by *Omega Engineering* with a maximum uncertainty of ≈ 30 Pa. The pressure drop was measured between inlet and front of a perforated plate, which is where the particles rest on. For each particle shape and inlet velocity the pressure drop measurements were repeated two times, whereby the bed was newly generated each time.

2.2 | Numerical methods

In the past years, several workflows have been proposed by different authors to conduct particle-resolved CFD simulations of fixed-bed reactors, as recently reviewed by Jurtz et al.¹⁰ What all workflows have in common is that they are based on the following four sequential steps: packing generation, CAD creation, meshing, and the actual CFD simulations. In this recent study, we use the approach developed by Eppinger et al.^{14,15} Here the bed is created by using DEM. Afterwards, position and orientation vectors of all particles are extracted and stored in a csv file. Based on this data, a CAD description of the packed bed is generated by placing CAD parts of the respective particle shape using JAVA macro functionality. As a final step the geometry is meshed. To avoid bad cells near particle-particle and particle-wall contacts, the local "caps" strategy is used¹⁴: during the meshing process an algorithm checks if CAD faces are in proximity to each other. If a certain distance is exceeded, the algorithm projects vertices along their connecting line and a small gap is introduced in the vicinity of the contact. The gap is filled with high quality volume cells. All numerical simulations are conducted with the commercial CFD tool *Simcenter STAR-CCM+* provided by *Siemens PLM Software*.

2.2.1 | Numerical packing generation

For numerical packing generation the discrete element method (DEM) established by Cundall and Strack²⁵ is used. This approach allows particles to overlap to a certain degree to calculate restitution and damping forces based on the overlap. The linear momentum equation for each particle is given by Newton's law of motion:

$$m_p \frac{dv_p}{dt} = \mathbf{F}_s + \mathbf{F}_b. \quad (2)$$

Here m_p and v_p are particle mass and velocity, t is time and \mathbf{F}_s and \mathbf{F}_b are the sum of surface and body forces that act on the particle.

For the filling process only the gravitational force and the contact forces are considered. The overall contact force is the sum of particle-particle and particle-wall contact forces acting on a particle, whereas each contact force can be decomposed in a tangential ($\mathbf{F}_{n,i}$) and a normal ($\mathbf{F}_{t,i}$) acting component:

$$\mathbf{F}_c = \sum_{i=0}^{\text{contacts}} (\mathbf{F}_{n,i} + \mathbf{F}_{t,i}). \quad (3)$$

The force in normal direction is defined by:

$$\mathbf{F}_n = -K_n d_n - N_n v_n. \quad (4)$$

Here K_n is the normal spring stiffness, d_n the overlap in normal direction, N_n the normal damping and v_n the normal velocity component of the relative sphere surface velocity at the contact point. The force in tangential direction is defined as:

$$\begin{cases} \mathbf{F}_t = -K_t d_t - N_t v_t & \text{for } |-K_t d_t| < |K_n d_n C_{fs}| \quad (\text{a}) \\ \frac{|K_n d_n| C_{fs} d_t}{|d_t|} & \text{for } |-K_t d_t| \geq |K_n d_n C_{fs}| \quad (\text{b}). \end{cases} \quad (5)$$

where K_t is the tangential spring stiffness, d_t the overlap in tangential direction, N_t the tangential damping, v_t the tangential velocity component of the relative sphere surface velocity at the contact point and C_{fs} the static friction coefficient.

In this study the non-linear Hertz-Mindlin contact model is used. This leads to:

$$K_n = \frac{4}{3} E_{\text{eq}} \sqrt{d_n R_{\text{eq}}} \quad (6)$$

$$K_t = 8 G_{\text{eq}} \sqrt{d_n R_{\text{eq}}} \quad (7)$$

$$N_n = N_{n,\text{damp}} \sqrt{5 K_n M_{\text{eq}}} \quad (8)$$

$$N_t = N_{t,\text{damp}} \sqrt{5 K_t M_{\text{eq}}}. \quad (9)$$

where $N_{n,\text{damp}}$ and $N_{t,\text{damp}}$ are the normal and tangential damping coefficients that are calculated from the normal and tangential restitution coefficient $C_{n,\text{rest}}$ and $C_{t,\text{rest}}$ as follows:

$$N_{n,\text{damp}} = \frac{-\ln(C_{n,\text{rest}})}{\sqrt{\pi^2 + \ln(C_{n,\text{rest}})^2}} \quad (10)$$

$$N_{t,\text{damp}} = \frac{-\ln(C_{t,\text{rest}})}{\sqrt{\pi^2 + \ln(C_{t,\text{rest}})^2}}. \quad (11)$$

M_{eq} , R_{eq} , E_{eq} , and G_{eq} are the equivalent values of mass, radius, Young's modulus, and shear modulus of particles A and B during the collision process:

$$M_{\text{eq}} = \frac{1}{\frac{1}{M_A} + \frac{1}{M_B}} \quad (12)$$

$$R_{\text{eq}} = \frac{1}{\frac{1}{R_A} + \frac{1}{R_B}} \quad (13)$$

$$E_{\text{eq}} = \frac{1}{\frac{1-\nu_A^2}{E_A} + \frac{1-\nu_B^2}{E_B}} \quad (14)$$

$$G_{\text{eq}} = \frac{1}{\frac{2(2-\nu_A)(1+\nu_A)}{G_A} + \frac{2(2-\nu_B)(1+\nu_B)}{G_B}} \quad (15)$$

where ν is the Poisson ratio.

Besides the linear, the angular momentum of each particle is conserved as well by:

$$I_p \frac{d\omega_p}{dt} = \sum_{i=0}^{\text{contacts}} (r_c \times F_{c,i} + M_{c,i}). \quad (16)$$

where I_p is the particle moment of inertia, ω_p the angular velocity, r_p the position vector from particles center of gravity to the contact point and M_c the acting moment due to rolling resistance:

$$M_c = -C_{\text{fr}} |r_c| |F_c| \frac{\omega_p}{|\omega_p|}. \quad (17)$$

Here C_{fr} is the rolling friction coefficient.

In its original form DEM is only applicable for the simulation of spherical particles. An approach to overcome this limitation is the use of composite (or glued) particles. By using the composite particle method, particles with complex shapes are approximated by an arrangement of spheres that are rigidly glued together. The composite particle representations of the particle shapes used in this study can be seen in Figure 1. A number of one-hundred spherical particles is used to approximate the real catalyst shape.

The particles inner voids are neglected for the filling simulation since it can be assumed that their impact on the particle dynamics is low. This is justified because of the small inner hole diameter which ensures that other particles cannot slide into them, and the axisymmetric nature of the investigated particle shape. Therefore, the center of mass of the pellet is not changed by neglecting the inner holes. Nevertheless, the particle mass is slightly increased if the inner holes are neglected. While particle sedimentation velocity is unaffected by particle mass, it has an impact on the calculated restitution forces during collision events. While the impact of frictional forces on bed voidage is widely accepted, only little data exists on the impact of particle mass or its density. Pottbäcker and Hinrichsen²⁶ studied experimentally the impact of different material properties on bed voidage and suspected that the coefficient of restitution and the particle density might affect the bed voidage. However, not all data fit to their hypothesis, for example, for spheres of rusty steel and polyoxymethylene the resulting bed voidage is equal, although, particle density is more than five times higher for steel, and static friction coefficients are similar. This indicates that the impact of particle density on bed voidage might be lower than expected. Hoffmann and Finkers²⁷ consolidated experimental data and derived a correlation for bed voidage as a function of sphericity, particle diameter, and particle density. However, the important frictional forces were not considered, and their data still shows scattering. Therefore, no clear conclusions

can be drawn. To understand the impact of particle density on bed voidage two additional DEM filling simulations were conducted. Five hundred cylindrical particles ($h = d_p = 16.5$ mm) are poured into a cylindrical container with a diameter of 101.6 mm. Randomly distributed injection points were placed at a height of 470 mm where particles enter the domain. Only gravitational and particle-particle and particle-wall contact forces were considered. Since in this case ideally cylindrical particles are considered the sophisticated contact detection method of Feng et al²⁸ in combination with the Linear Spring Contact Model was used. All boundary conditions and material properties except for the particle density are equal. As reference case a particle density of 2,200 kg/m³ was used. For the second simulation this value was reduced to 1,100 kg/m³. This is comparable to simulating particles with 50% inner voids but neglecting the additional voidage in the DEM simulation. The result of this preliminary study is given in Figure 3. For better visibility the highest and lowest particle position of the last particle layer are marked for both cases. Almost no difference can be observed, which shows that impact of particle density on bed voidage can be neglected. However, it needs to be mentioned that this statement cannot be generalized and is only true, if hole diameters are small. For shapes with large voids, as thin-walled rings, neglecting the inner void during DEM simulation can lead to significant deviations regarding particle orientation and radial void fraction distribution as recently shown.²⁹

The bed voidage between the experimental and numerical packing has to be in good agreement for an accurate prediction of pressure drop. However, very often not all important aspects concerning the

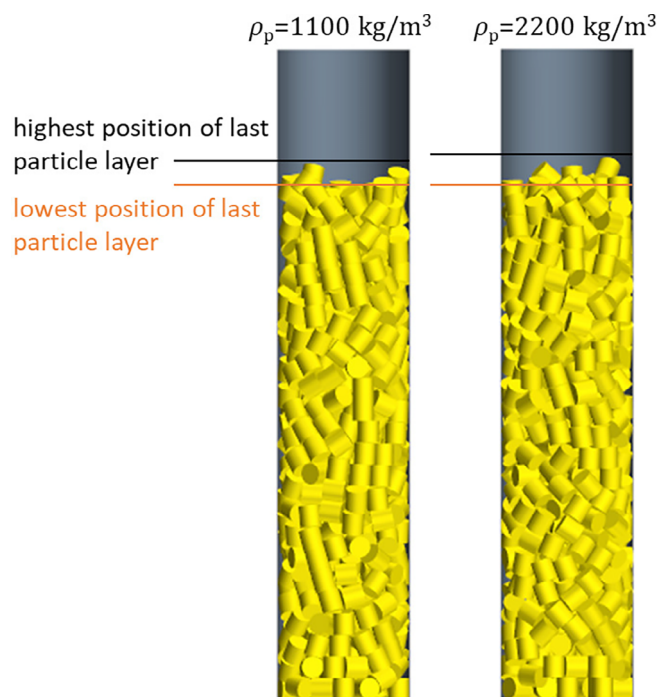


FIGURE 3 Impact of particle density on bed height for cylinders in a bed with a tube-to-particle diameter ratio of $N = 5.4$ [Color figure can be viewed at wileyonlinelibrary.com]

filling process are known. The surface characteristics of the particle (esp. the static friction coefficient) is mostly unknown and vibrations or artificial densification (e.g., hammering) has a huge impact on the bed voidage as well. Ookawara et al.¹⁷ found that the static friction coefficient can be used to fine-tune the packing density to the desired experimental value. Recently, Jurtz et al.²⁴ have proposed correlations to predict bed voidage as a function of tube-to-particle diameter ratio and static friction coefficient for spheres, cylinders, and Raschig rings. These equations can be used to pre-calculate the friction coefficient to achieve a certain bed voidage. It should be noted that other parameters, such as filling speed, may also impact the final bed voidage, as recently shown by Fernengel et al.³⁰

Within the scope of this work the static friction coefficient is first manually adapted using trial-and-error method until the numerical and experimental bed voidage is in acceptable agreement. The loading device is neglected in that simulations. Subsequently, the pressure drop is calculated and compared with experimental results. In the second part of this study, it is investigated if, in analogy to the work of Jurtz et al.,²⁴ it is possible to obtain a correlation for more complex catalyst shapes with a set of DEM simulations and just one filling experiment. To ensure that the correlation only accounts for frictional and vibration effects the loading device will be considered in these simulations.

To include the CATCADE™ loading device in the filling simulation, as depicted in Figure 4a, the overset mesh approach is used. This method often called chimera grid method was first introduced by Steger et al.³¹ and Benek et al.^{32,33} It allows the spatial discretization of the numerical domain by two or even more intersecting mesh topologies. The main topology, often called the background domain, encloses the static region and includes only the outer boundaries of the domain. In the present case the background mesh is represented by the cylindrical reactor tube. The second region is often called the overset domain and includes movable boundaries, here the loading device, plus an outer boundary that is named the overset interface.

After each time step the hole-cutting process is started and based on the position of the overset interface holes are cut in the background mesh. Along the overset interface, a layer of cells is identified that forms the donor cell layer. The cells of the background mesh next to the donor cell layer become acceptor cells. They have to form a watertight boundary around the overset region. Cells of the background mesh that are completely covered by the overset region cells inside this closed boundary become deactivated. For each acceptor cell a donor cell must be found to couple the overset and background mesh. The cell status for overset and background mesh as well as a visualization of the final mesh can be seen in Figure 4b.

The movement of the loading device is implemented as a translational motion in vertical direction as visualized in Figure 4c. To check the current bed height during the DEM simulation a threshold is created that includes all particles that have a minimum number of three adjacent particles they are in contact with. The maximum vertical coordinate of the threshold is evaluated as current bed height. If the distance between bottom of the loading device and the bed surface falls below a value of 5 cm the device is moved upwards with a constant velocity of 0.15 m/s. Particles are injected with a randomly distributed initial orientation at a height of 2.5 m.

2.2.2 | Computational fluid dynamics

For the flow simulations mass and momentum conservation equation is solved using the Finite Volume Method (FVM):

$$\frac{\partial \rho}{\partial t} + \nabla \cdot (\rho \mathbf{v}) = 0 \quad (18)$$

$$\frac{\partial (\rho \mathbf{v})}{\partial t} + \nabla \cdot (\rho \mathbf{v} \mathbf{v}) = \nabla T \quad (19)$$

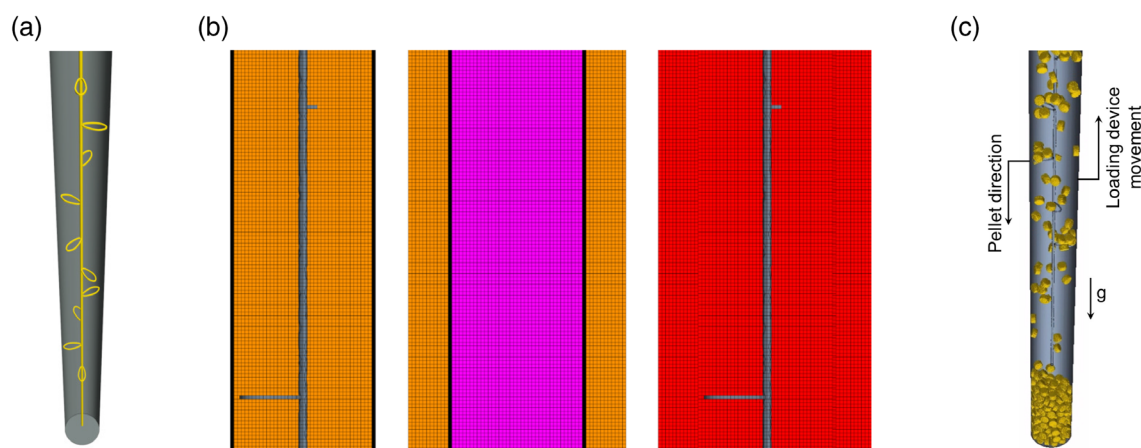


FIGURE 4 Inclusion of the loading device. (a) CAD description. (b) Visualization of overset mesh (left), background mesh (middle) and final mesh (right). Cells of overset and background mesh are colored by their cell status (magenta: inactive cells, black: donor and acceptor cells, orange: active cells). (c) Still of the filling process (an animation is provided in the Video S1) [Color figure can be viewed at wileyonlinelibrary.com]

Here ρ is mass density of the fluid, \mathbf{v} fluid velocity, and \mathbf{T} the stress tensor:

$$\mathbf{T} = -\left(p + \frac{2}{3}\mu\nabla \cdot \mathbf{v}\right)\mathbf{I} + 2\mu\mathbf{D}, \quad (20)$$

where p is pressure, μ dynamic viscosity, \mathbf{I} the unit tensor, and \mathbf{D} the deformation tensor:

$$\mathbf{D} = \frac{1}{2}[\nabla\mathbf{v} + (\nabla\mathbf{v})^T]. \quad (21)$$

Turbulent effects are considered by using the Realizable k - ϵ turbulence model which has already successfully been used in previous studies.^{14,15,18} The steady-state solution is solved by using an incompressible segregated solver approach. The SIMPLE-algorithm is used to solve for the pressure-velocity coupling.

The numerical domain is spatially discretized using polyhedral cells as depicted in Figure 5. In order to avoid insufficient mesh quality at particle contacts, the caps method introduced by Eppinger et al¹⁴ was applied, which creates small gaps between touching particles. The approach is fully automatized and can be applied to any type of particle shape without additional modification.¹⁰ In comparison to other contact modification methods (e.g., bridging particle contacts) it can directly be applied for heat transfer simulations without having to specify an additional thermal resistance at the contacts.¹⁹ A detailed mesh refinement study was recently published by Minhua et al.³⁴ Two prism layers are used to resolve velocity gradients at the particle surface and reactor wall. In order to minimize the influence of the

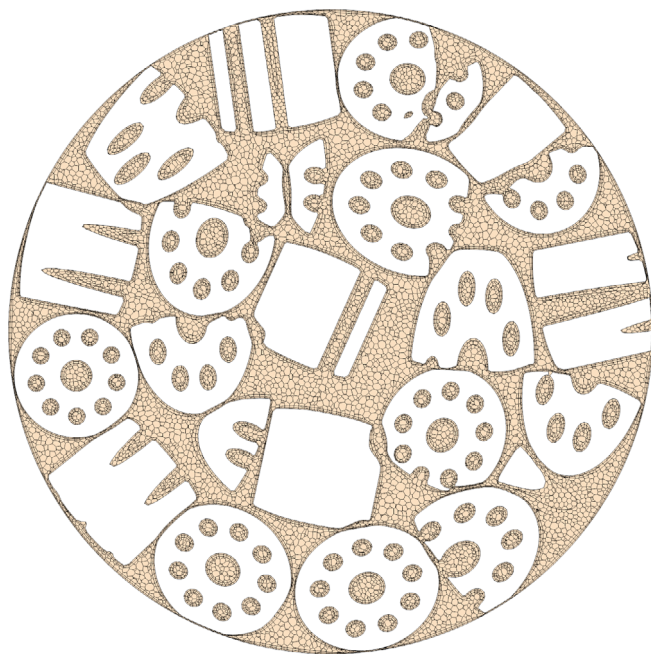


FIGURE 5 Projection of the polyhedral mesh on a cross-sectional plane for LDP shape [Color figure can be viewed at wileyonlinelibrary.com]

boundary conditions at the inlet and outlet, the volume mesh is extended by extruding the inlet and outlet. The total cell count was 9.1 million for Raschig rings and around 11.5 million for LDP and FD shape. The overall mesh quality is reasonably good for such complex geometries. A maximum of one out of ten thousand cells have a least square cell quality below 0.001. This metric is an indicator of the quality of a cell, using the physical location of a cell centroid relative to the cell centroid locations of its face-neighbors.³⁵

3 | RESULTS

3.1 | Pressure drop

The pressure drop of packed beds with a bed height of $H = 445.0$ mm and a diameter of $D = 101.6$ mm were investigated numerically and experimentally for Raschig rings, LDP 19×16 and FD particle shape. Since pressure drop is very sensitive to bed voidage, it is essential that the difference in bed voidage is as low as possible between the numerical packing and its experimental counterpart. Therefore, the static friction coefficient was adapted using trial-and-error to a value of $C_{fs} = 0.02$ in the DEM simulation to meet the experimental bed voidage. A comparison between the experimental and numerical values in terms of particle count and bed voidage can be found in Table 2, whereby inner particle voids were considered to calculate the bed voidage. A very good agreement with the experimentally determined particle count can be observed for all three particle shapes. A maximum error of 1.4% can be found for Raschig rings.

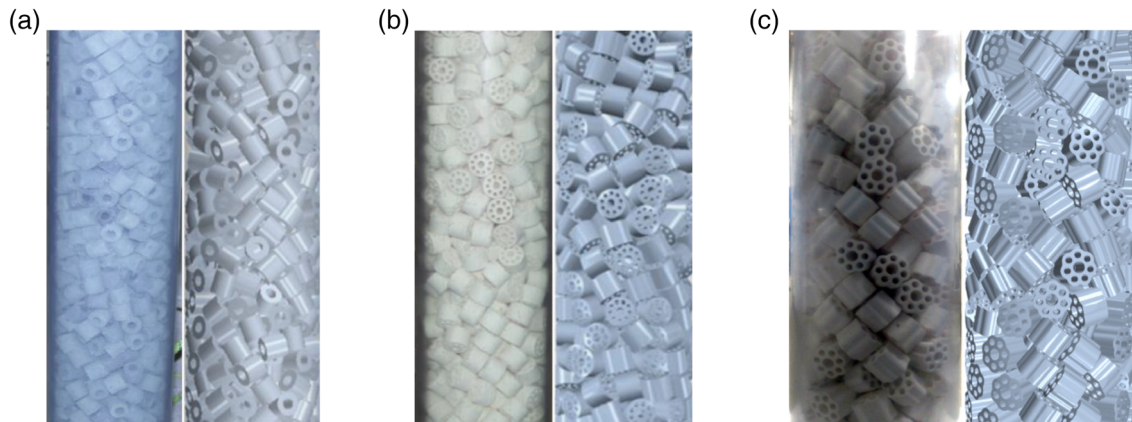
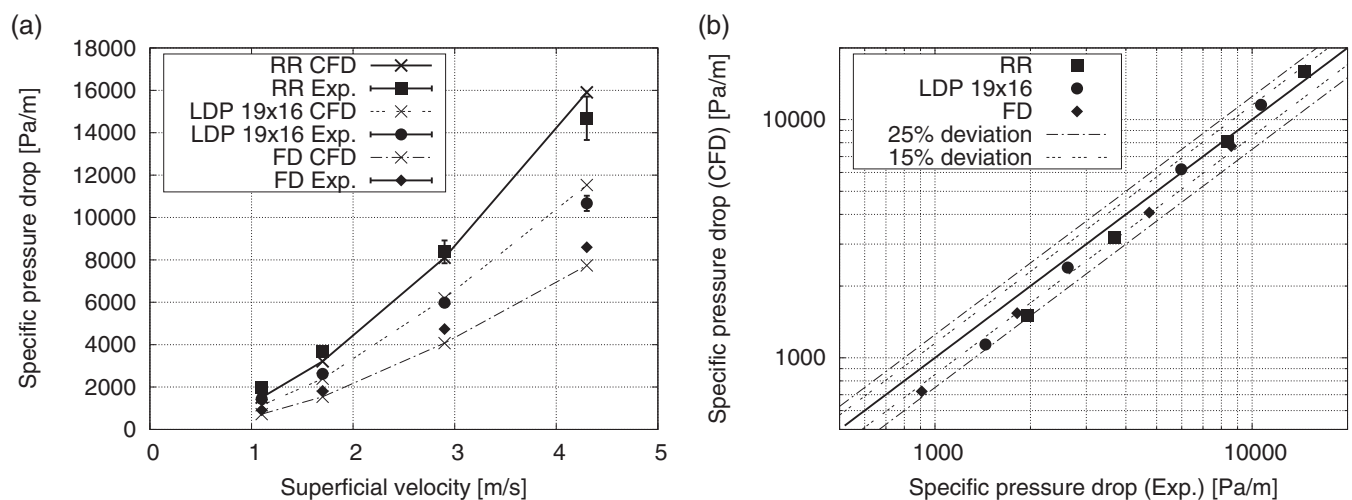
In Figure 6 the experimental and numerical packing are visually compared. It can be seen that at the reactor wall the particle orientation is qualitatively in a good agreement. The majority of particles are either aligned orthogonally or in parallel to the reactor wall. There is also a trend of building stacked structures, which is something that Zhang et al³⁶ already noticed in their packing experiments with equilateral cylinders.

For each of the packings, several flow simulations with varying inlet velocities (1.1, 1.7, 2.9, and 4.3 m/s) were conducted. This corresponds to a range of investigated particle Reynolds numbers of $Re_p = (v_{in} \cdot d_p \cdot \rho)/\mu \approx 1300$ -5800. A constant fluid density of $\rho = 1.19$ kg/m³ and a fluid dynamic viscosity of $\mu = 1.8326 \times 10^{-5}$ Pa s was used for these simulations. The comparison between experimentally determined specific pressure drop plus its standard deviation and simulation results is given in Figure 7a. The same trend is predicted by experiments and numerical simulations: the largest pressure drop can be observed for Raschig rings followed by the LDP 19×16 and the FD particle shape. For the same superficial inlet velocity the pressure drop can be cut in half by using the FD particle shape. The parity plot in Figure 7b shows the accuracy of calculated pressure drop in comparison to the experimental values. For almost all configurations the deviation is below 15% which is within the accuracy that Eppinger et al¹⁴ reported for spherical particles. However, for the lowest inlet velocity the pressure drop is slightly

TABLE 2 Comparison of particle count and void fraction for experimentally and numerically generated packings

	RR		LDP 19 × 16		FD	
	DEM	Exp.	DEM	Exp.	DEM	Exp.
Particle count (-)	660	668	505	502	457	454
Bed voidage (-)	0.489	0.482	0.542	0.545	0.623	0.627

Abbreviations: DEM, discrete element method; RR, Raschig rings.

**FIGURE 6** Comparison between experimental (left) and numerical (right) bed structure: (a) Raschig ring, (b) LDP 19 × 16, and (c) FD shape [Color figure can be viewed at wileyonlinelibrary.com]**FIGURE 7** Pressure drop results: (a) Specific pressure drop as a function of superficial velocity and (b) parity plot for comparison of experimental and numerical results

underestimated, leading to deviations between 20% for FD shape and 23% for Raschig rings.

3.2 | Impact of loading device on bed voidage and particle orientation

In the previous simulations, the loading device was not used, neither in the experiment nor in the simulation. Since it is usually used during

the experimental filling procedure, the question is raised, if this is a valid assumption or if the device should be considered when it is used. To answer this question several loading simulations of LDP 19 × 12 particles were performed and the impact of the loading device on particle orientation was investigated by conducting simulations with and without the loading device. The static friction coefficient was varied from $C_{fs} = 0.001-0.8$ to investigate the impact of the loading device for different packing densities. With increasing friction coefficient the generated packing becomes more loose. The orientation of each

particle is evaluated with respect to the angle between its symmetry axis and the normal vector on the horizontal plane.

The results given in Figure 8 show that for almost all packings the majority of particles have an orientation with respect to the horizontal plane of 80–90°. This is in good agreement with the experimental results of Caulkin et al.²² who also found that cylindrical particles tend to arrange orthogonally to the horizontal plane. A good agreement can be found between the simulation results and the experimental data of Caulkin et al.²² for static friction coefficients in the range $C_{fs} = 0.4$ –0.8. With decreasing friction coefficient (denser beds) the amount of orthogonally and horizontally aligned particles increase significantly when the loading device is used. The number of particles with an orientation of 30–70° are reduced. For dense beds, about 50% of the particles are either horizontally or vertically aligned when the loading device is used.

Without the loading device the change in particle orientation is less continuous and an abrupt reduction of orthogonally aligned particles can be recognized if the friction coefficient is set to a value of $C_{fs} \geq 0.4$. The trend of a reduced number of diagonal particle alignment is less pronounced in comparison to the results where the loading device was included. In the case of very dense beds only about 40% of the particles are horizontally or vertically aligned.

A direct comparison of particle orientation with and without the loading device for different friction coefficients can be seen in Figure 9. For very dense and loose bed configurations an impact of the loading device on particle orientation can be observed. For very low friction coefficients of $C_{fs} \leq 0.1$ the number of particles that have an orientation angle of 90° is increased by up to 20%. Increasing the static friction coefficient to values $C_{fs} \geq 0.6$ causes the opposite effect: the number of orthogonally aligned particles is reduced by up to 25%. It cannot be seen that the change in orthogonally aligned particles leads to any different preferred orientation angle. Regardless of

whether the loading device is used or not, with increasing friction coefficients the particle orientation distribution gets more uniform, although, particles with an orientation angle below 30° are always underrepresented.

Besides particle orientation also bed voidage is affected by the loading device as it can be seen in Figure 10. For different values of static friction coefficient the bed voidage is given and compared with the correlation of Dixon³⁷ and Foumeny and Benyahia.³⁸ Here, inner particle voids are not considered to calculate the bed voidage to ensure a better comparability with the presented correlations. It can be seen that the use of the loading device leads to a significantly increased bed voidage for friction coefficients $C_{fs} > 0.05$. Below this value only slight differences in void fraction can be observed and the calculated values agree well with those predicted by the correlation of Foumeny and Benyahia³⁸ for dense beds. For friction coefficients in the range of $C_{fs} = 0.4$ –0.8 which is in the order of magnitude of most catalyst supports as alumina or silicon carbide³⁹ the results of the simulation without the loading device are in good agreement with the predicted values of the correlation of Dixon³⁷ for non-densified beds. However, it can be seen that the use of the loading device leads to a significant increase in bed voidage of up to 10%. This effect can mainly be attributed to a reduction of dropping height or reduced impact velocity caused by the loading device. Li⁴⁰ investigated the impact of dropping height on bed voidage for ellipsoids and found for particles with moderate aspect ratios of 0.5–2.0 a comparable increase in bed voidage if dropping height is reduced under a certain limit. With increasing aspect ratio, the effect gets less pronounced due to the increasing amount of kinetic energy that is dissipated by particle-particle friction. Overall, the results show that whenever loading devices are used they should also be considered in the numerical filling simulation since they strongly affect particle orientation and bed voidage.

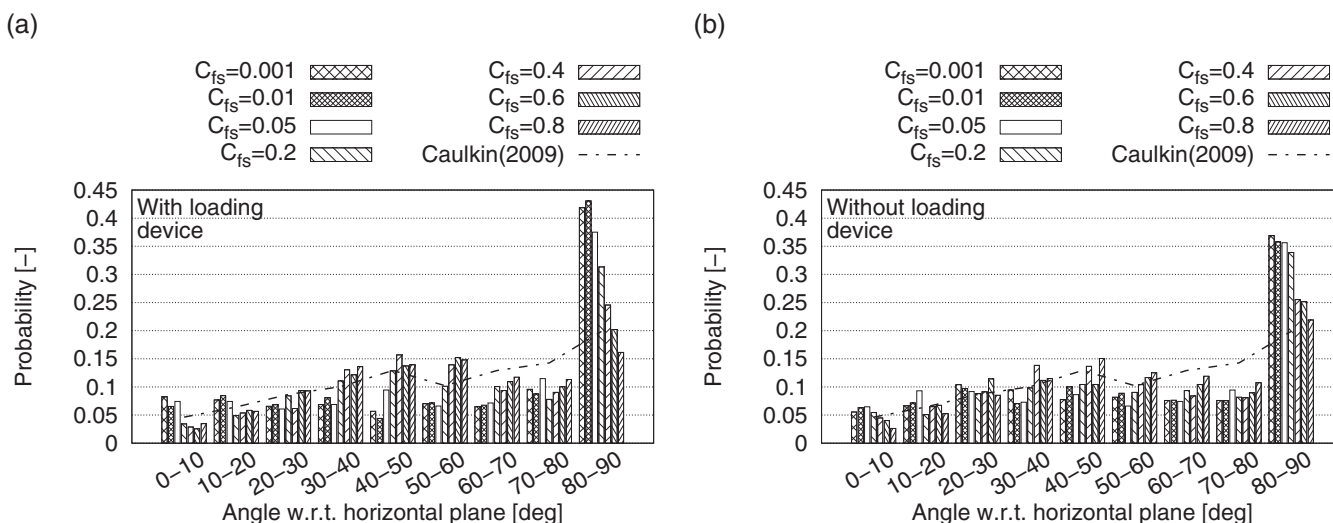


FIGURE 8 Impact of static friction coefficient on particle orientation for LDP 19 × 12 shape: (a) With loading device and (b) without loading device

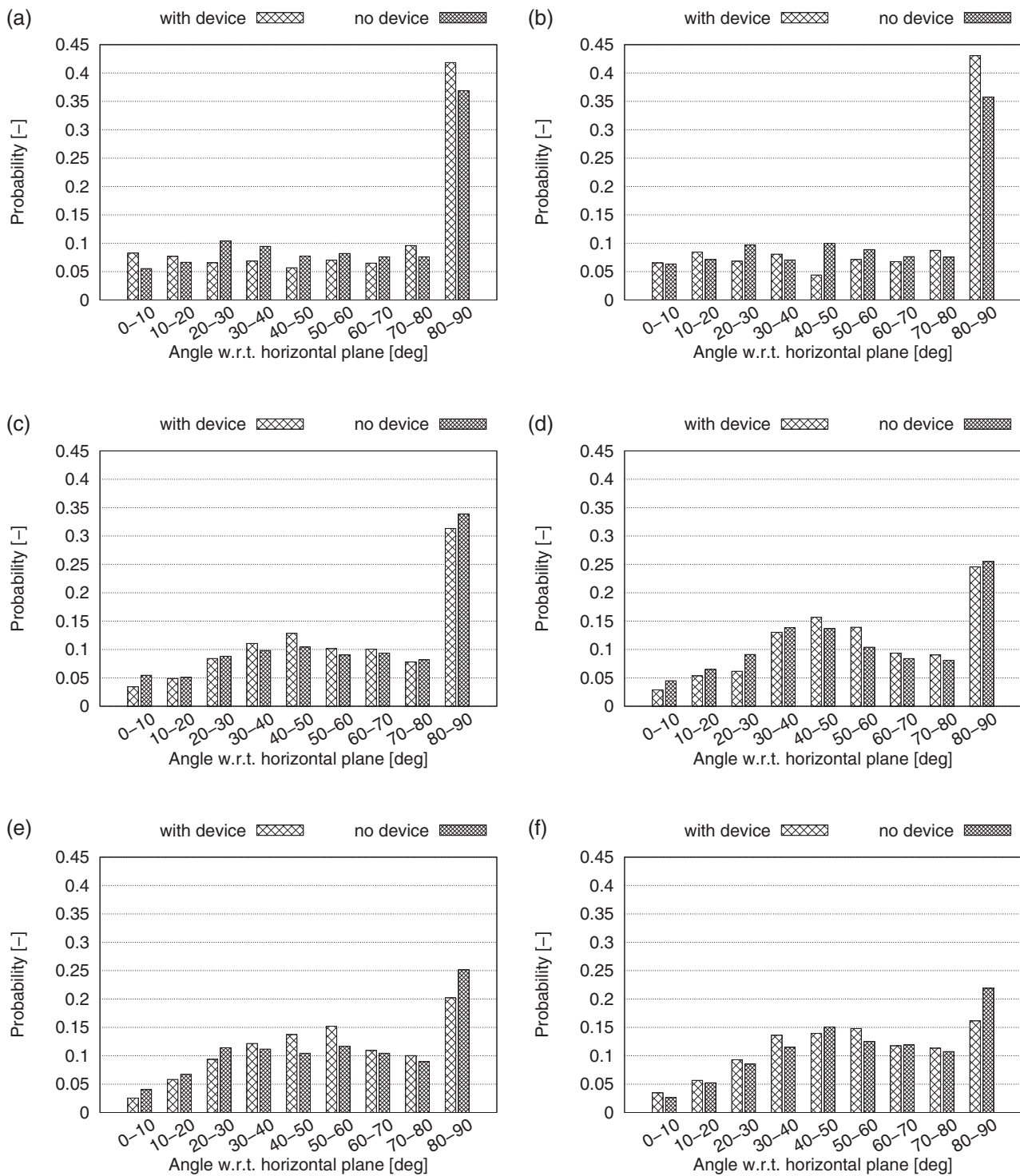


FIGURE 9 Impact of loading device on particle orientation for LDP 19×12 shape: (a) $C_{fs} = 0.001$, (b) $C_{fs} = 0.01$, (c) $C_{fs} = 0.2$, (d) $C_{fs} = 0.4$, (e) $C_{fs} = 0.6$, and (f) $C_{fs} = 0.8$

4 | DISCUSSION

It was shown that the particle-resolved CFD approach is in general able to predict fluid dynamics accurately as long as bed voidage of the experimental and numerical packing are equal. As already discussed bed voidage strongly depends on experimental filling procedure

(e.g., artificial tamping and the use of loading devices) as well as surface characteristics of the particles. Loading devices can explicitly be included in the filling simulation as shown and lead to an increase of bed voidage and can also cause a change of particle orientation close to the reactor wall. However, most often the static friction coefficient for the respective system is unknown and artificial tamping is used to

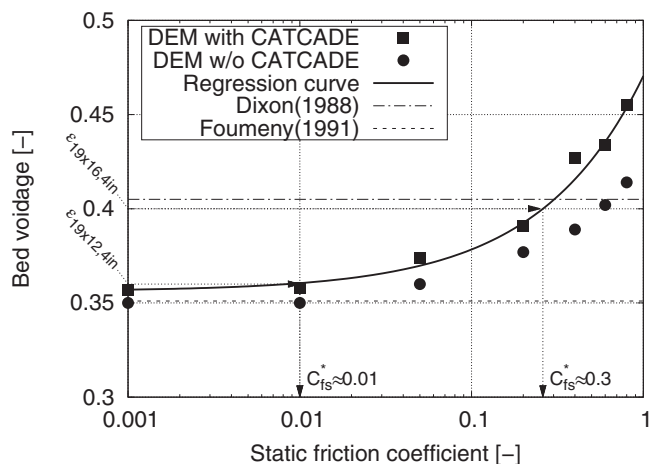


FIGURE 10 Calibration curve for LDP 19×12 and impact of loading device on bed voidage

create dense beds. This arises the question what value for the static friction coefficient should be used in the DEM simulation to generate a packing that is in good agreement with the experimental one by considering these effects.

It was recently shown by Jurtz et al²⁴ that the effect of tamping and surface characteristics can be lumped into the static friction coefficient and that it is possible to generate packings with a desired bed voidage by using an adapted friction coefficient. Nevertheless, their investigations were limited to simple particle shapes as cylinders, hollow-cylinders and spheres, and the question remained if a once calibrated friction factor can be used to predictively describe the bed voidage of other reactor configuration with the same type of particles. If this is possible it would be a straight forward method for the calibration of the friction coefficient since just one experimental filling and some DEM simulations would be necessary.

To investigate this, a packing of 19×12 LDP particles in a 4''-tube was generated in the lab. The loading device was used during the filling process and the number of particles within a bed height of $H = 457.2$ mm were counted. Based on the numerical results shown in Figure 10 a regression curve was fitted. Based on that function and the experimentally bed voidage $\epsilon_{19 \times 12, 4}$ in the static friction coefficient of the respective particle shape was calibrated to a value of $C_{fs} = 0.01$. With the adapted friction coefficient filling simulations of 19×12 LDP particles in 4''- and 6''-tubes were conducted and compared with experimental measurements as shown in Figure 11. A bed height of $H = 508.0$ mm was used for the 6''-tube. In case of the 4''-tube the experimental and numerical particle count is almost identical which is not unexpected since this was the reference case for the calibration of the friction coefficient. Nevertheless, the results for the 6''-tube also show very good agreement between experimental particle count and simulation result with an error in terms of particle count below 1%. This indicates that with a once calibrated friction coefficient bed voidage of reactors with different tube-to-particle diameter ratios can be predicted using DEM. This brings particle-resolved CFD

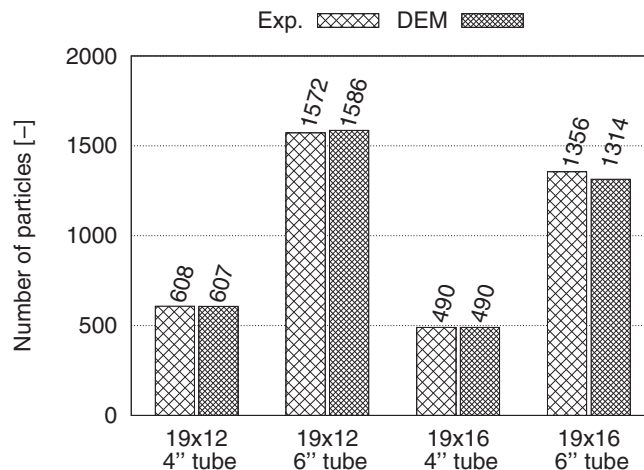


FIGURE 11 Comparison of experimental and numerical particle count for 19×12 LDP ($C_{fs} = 0.01$) and 19×16 LDP shape ($C_{fs} = 0.3$) for different tube diameters

one step further toward being a predictive design tool for new catalyst shapes. A potential work flow could be as follows:

1. For a new particle shape a series of DEM simulations with different values for the static friction coefficient are conducted. If needed, a loading device can be included in the DEM simulation to account for its effect explicitly.
2. A regression curve is fitted based on the numerical data of the bed voidage.
3. A filling experiment with a certain tube-to-particle diameter ratio is conducted and bed voidage is evaluated.
4. Based on the numerical regression curve and the experimentally measured bed voidage the static friction coefficient is calibrated.
5. The calibrated static friction coefficient can be used for filling simulations in the particle-resolved CFD framework to predictively generate packing geometries for different tube-to-particle diameter ratios under same filling conditions.

A good description of bed morphology is of major importance for an accurate prediction of fluid dynamics, heat/mass transfer and chemical reactions by particle-resolved CFD simulations. The proposed work flow significantly reduces the numerical turnaround time and experimental effort to generate packing geometries that are comparable to its experimental/industrial counterpart.

The experiments and simulations were repeated for 19×16 LDP shapes using $C_{fs} = 0.01$ to evaluate if the determined static friction coefficient can also be used for slightly modified particle shapes. However, the simulation results have shown an up to 9% higher particle count than the one that was found in experiments. Therefore, based on the already existing calibration curve for 19×12 LDP given in Figure 10, the static friction coefficient was adapted to a value of $C_{fs} = 0.3$ which corresponds to the experimentally determined bed voidage for 19×16 LDP in 4''-tube of $\epsilon_{19 \times 16, 4}$ in. The DEM

simulations were repeated with the adapted friction coefficient. The comparison to experimental data is given in Figure 11 and shows good agreement between experimentally and numerically generated packings. For the 4"-tube the simulation results exactly match the experimental data, while for the 6"-tube the particle count is underestimated by 3%. This may indicate that an existing calibration curve, to some extent, can also be used if particle geometry is slightly modified, for example, small changes in aspect ratio. This is in accordance with results of Jurtz et al.²⁴ who found for cylindrical particles only little effect of aspect ratio on bed voidage if $0.5 < h/d_p < 2$. Nevertheless, further experimental and numerical investigations are needed to assess the validity and accuracy when using a calibration curve for modified particle shapes, especially for those with additional outer surface structure.

5 | CONCLUSION

Particle-resolved CFD was applied to simulate the fluid dynamics in packed-beds filled with different complex particle shapes over a wide range of industrially relevant Reynolds numbers ($Re_p \approx 1300$ -5800). It was shown that an accurate prediction of pressure drop with a deviation in the range of $\pm 15\%$ can be achieved if bed voidage is in agreement with the experimentally investigated packing. The particle orientation close to the reactor wall was also found to be qualitatively in accordance with lab results.

For the first time the impact of loading devices on particle orientation and bed voidage was studied numerically. It was found that bed voidage is significantly increased if loading devices are used. Therefore, it is advised to explicitly include them in the packing generation simulation. It was shown that the overset mesh approach is an efficient and reliable method to include moving boundaries in the simulation.

Since it is of major importance to meet the bed voidage as close as possible, it was shown how this can be efficiently achieved, and experimental and numerical effort can be minimized. It is proposed to use an adapted static friction coefficient to account for artificial densification and surface characteristics. A once calibrated friction coefficient can be used to simulate reactor configurations that differ in tube-to-particle diameter ratio as long as the same filling strategy is used.

NOTATION

ω_p	particle angular velocity, rad/s
D	deformation tensor, 1/s
F_b	body forces, N
F_n	normal contact force, N
F_s	surface forces, N
F_t	tangential contact forces, N
I_p	particle moment of inertia, kg/m^2
I	unit tensor, (-)
M_c	moment due to contact, N m

r_p	position vector from particle center of gravity to contact point, m
T	stress tensor, Pa
v_p	particle velocity, m/s
v	fluid velocity, m/s
μ	dynamic viscosity, Pa s
ν	Poisson ratio, (-)
ρ	fluid density, kg/m^3
C_{fr}	rolling friction coefficient, (-)
C_{fs}	static friction coefficient, (-)
$C_{n, rest}$	normal restitution coefficient, (-)
$C_{t, rest}$	tangential restitution coefficient, (-)
D_i	inner tube diameter, m
d_n	overlap in normal direction, m
$d_{p, i}$	inner diameter, m
$d_{p, o}$	outer diameter, m
d_p	sphere-equivalent particle diameter, m
d_t	overlap in tangential direction, m
E_{eq}	particle equivalent Young's modulus, Pa
G_{eq}	particle equivalent shear modulus, Pa
H	bed height, m^3
h	particle height, m
i	contact index, (-)
K_n	normal spring stiffness, N/m
K_t	tangential spring stiffness, N/m
M_{eq}	particle equivalent mass, kg
m_p	particle mass, kg
N	tube-to-particle diameter ratio, (-)
$N_{n, damp}$	normal damping coefficient, (-)
N_n	normal damping, N s/m
$N_{t, damp}$	tangential damping coefficient, (-)
N_t	tangential damping, N s/m
p	pressure, Pa
R_{eq}	particle equivalent radius, m
t	time, s
v_n	normal velocity component of the relative sphere surface velocity, m/s
V_p	particle volume, m^3
v_t	tangential velocity component of the relative sphere surface velocity, m/s

ORCID

Nico Jurtz  <https://orcid.org/0000-0003-0426-6159>

REFERENCES

1. Aasberg-Petersen K, Dybkjær I, Ovesen C, Schjødt N, Sehested J, Thomsen S. Natural gas to synthesis gas-catalysts and catalytic processes. *J Nat Gas Sci Eng.* 2011;3(2):423-459.
2. Bruno SP, Barreto GF, Gonzalez MG. Effect of the geometric characteristics of commercial catalysts for steam reforming. *Chem Eng J.* 1988;39(3):147-156.
3. Sie S, Krishna R. Process development and scale up: II. Catalyst design strategy. *Rev Chem Eng.* 1998;14(3):159-202.

4. Afandizadeh S, Foumeny E. Design of packed bed reactors: guides to catalyst shape, size, and loading selection. *Appl Therm Eng.* 2001;21(6):669-682.
5. Kagymanova A, Zolotarskii I, Smirnov E, Vernikovskaya N. Optimum dimensions of shaped steam reforming catalysts. *Chem Eng J.* 2007;134(1-3):228-234.
6. Hartmann V, Obysov A, Dulnev A, Afanas'ev S. New basic shape of catalysts for natural gas reforming reactors. *Chem Eng J.* 2011;176:102-105.
7. Franczyk E, Gołębowski A, Borowiecki T, Kowalik P, Wróbel W. Influence of steam reforming catalyst geometry on the performance of tubular reformer-simulation calculations. *Chem Process Eng.* 2015;36(2):239-250.
8. Karthik G, Buwa VV. A computational approach for the selection of optimal catalyst shape for solid-catalysed gas-phase reactions. *React Chem Eng.* 2020;5:163-182.
9. Dixon AG, Nijemeisland M, Stitt EH. Packed tubular reactor modeling and catalyst design using computational fluid dynamics. *Adv Chem Eng.* 2006;31:307-389.
10. Jurtz N, Kraume M, Wehinger GD. Advances in fixed-bed reactor modeling using particle-resolved computational fluid dynamics (CFD). *Rev Chem Eng.* 2019;35(2):139-190.
11. Augier F, Idoux F, Delenne JY. Numerical simulations of transfer and transport properties inside packed beds of spherical particles. *Chem Eng Sci.* 2010;65(3):1055-1064.
12. Xu C, Jia X, Williams R, et al. Property predictions for packed columns using random and distinct element digital packing algorithms. *Fifth World Congress on Particle Technology.* Orlando, FL: Citeseer; 2006.
13. Caulkin R, Jia X, Xu C, et al. Simulations of structures in packed columns and validation by X-ray tomography. *Ind Eng Chem Res.* 2008;48(1):202-213.
14. Eppinger T, Seidler K, Kraume M. DEM-CFD simulations of fixed bed reactors with small tube to particle diameter ratios. *Chem Eng J.* 2011;166(1):324-331.
15. Eppinger T, Jurtz N, Aglave R. Automated workflow for spatially resolved packed bed reactors with spherical and non-spherical particles. In: *10th International Conference on CFD in Oil & Gas, Metallurgical and Process Industries. SINTEF, Trondheim, Norway.* 2014:1-10.
16. Boccardo G, Augier F, Haroun Y, Ferre D, Marchisio DL. Validation of a novel open-source work-flow for the simulation of packed-bed reactors. *Chem Eng J.* 2015;279:809-820.
17. Ookawara S, Kuroki M, Street D, Ogawa K. High-fidelity DEM-CFD modeling of packed bed reactors for process intensification. In: *Proceedings of European Congress of Chemical Engineering (ECCE-6), Copenhagen;* 2007:16-20.
18. Wehinger GD, Eppinger T, Kraume M. Detailed numerical simulations of catalytic fixed-bed reactors: Heterogeneous dry reforming of methane. *Chem Eng Sci.* 2015;122:197-209.
19. Wehinger GD, Fütterer C, Kraume M. Contact modifications for CFD simulations of fixed-bed reactors: cylindrical particles. *Ind Eng Chem Res.* 2016;56(1):87-99.
20. Dong Y, Sosna B, Korup O, Rosowski F, Horn R. Investigation of radial heat transfer in a fixed-bed reactor: CFD simulations and profile measurements. *Chem Eng J.* 2017;317:204-214.
21. Dong Y, Geske M, Korup O, et al. What happens in a catalytic fixed-bed reactor for n-butane oxidation to maleic anhydride? Insights from spatial profile measurements and particle resolved CFD simulations. *Chem Eng J.* 2018;350:799-811.
22. Caulkin R, Ahmad A, Fairweather M, Jia X, Williams R. Digital predictions of complex cylinder packed columns. *Comput Chem Eng.* 2009;33(1):10-21.
23. Caulkin R, Jia X, Fairweather M, Williams RA. Predictions of porosity and fluid distribution through nonspherical-packed columns. *AIChE J.* 2012;58(5):1503-1512.
24. Jurtz N, Waldherr P, Kraume M. Numerical analysis of the impact of particle friction on bed voidage in fixed-beds. *Chem Ing Tech.* 2019;91(9):1260-1266.
25. Cundall PA, Strack OD. A discrete numerical model for granular assemblies. *Geotechnique.* 1979;29(1):47-65.
26. Pottbäcker J, Hinrichsen O. Experimental study on the influence of filling method and particle material on the packed-bed porosity. *Chem Ing Tech.* 2017;89(4):454-458.
27. Hoffmann A, Finkers H. A relation for the void fraction of randomly packed particle beds. *Powder Technol.* 1995;82(2):197-203.
28. Feng Y, Han K, Owen D. A generic contact detection framework for cylindrical particles in discrete element modelling. *Comput Methods Appl Mech Eng.* 2017;315:632-651.
29. Flaischlen S, Wehinger GD. Synthetic packed-bed generation for CFD simulations: blender vs. STAR-CCM+. *ChemEngineering.* 2019;3(2):52.
30. Fernengel J, von Seckendorff J, Hinrichsen O. Influence of cylinder-to-particle diameter ratio and filling speed on bed porosity of random packed beds of spheres. *Comput Aided Chem Eng.* 2018;43:97-102.
31. Steger JL, Dougherty FC, Benek JA. A chimera grid scheme.[multiple overset body-conforming mesh system for finite difference adaptation to complex aircraft configurations]. In: *Advances in grid generation; Proceedings of the Applied Mechanics, Bioengineering, and Fluids Engineering Conference;* 1983:59-69.
32. Benek J, Steger J, Dougherty FC. A flexible grid embedding technique with application to the Euler equations. In: *6th Computational Fluid Dynamics Conference Danvers;* 1983: AIAA Paper No. 83-1944.
33. Benek J, Buning P, Steger J. A 3-D chimera grid embedding technique. In: *7th Computational Physics Conference.* 1985; pp. AIAA Paper No. 85-1523.
34. Minhua Z, He D, Zhongfeng G. A particle-resolved CFD model coupling reaction-diffusion inside fixed-bed reactor. *Adv Powder Technol.* 2019;30(6):1226-1238.
35. *STAR-CCM+ User Guide Version (14.02).* Siemens PLM Software Inc; 2019.
36. Zhang W, Thompson KE, Reed AH, Beenken L. Relationship between packing structure and porosity in fixed beds of equilateral cylindrical particles. *Chem Eng Sci.* 2006;61(24):8060-8074.
37. Dixon AG. Correlations for wall and particle shape effects on fixed bed bulk voidage. *Can J Chem Eng.* 1988;66(5):705-708.
38. Foumeny E, Benyahia F. Predictive characterization of mean voidage in packed beds. *Heat Recovery Syst CHP.* 1991;11(2-3):127-130.
39. Pasaribu H, Sloetjes J, Schipper D. Friction reduction by adding copper oxide into alumina and zirconia ceramics. *Wear.* 2003;255:699-707.
40. Li C. Experimental and simulation study on packing of spherical and ellipsoidal particles. [PhD thesis]. University of New South Wales. Materials Science & Engineering; 2014.

SUPPORTING INFORMATION

Additional supporting information may be found online in the Supporting Information section at the end of this article.

How to cite this article: Jurtz N, Wehinger GD, Srivastava U, Henkel T, Kraume M. Validation of pressure drop prediction and bed generation of fixed-beds with complex particle shapes using discrete element method and computational fluid dynamics. *AIChE J.* 2020;66:e16967. <https://doi.org/10.1002/aic.16967>